
KEMP-PIP: A FEATURE-FUSION BASED APPROACH FOR PRO-INFLAMMATORY PEPTIDE PREDICTION

Soumik Deb Niloy[†]

Department of Computer Science and Engineering
BRAC University
Dhaka 1212, Bangladesh
soumik.deb.niloy@g.bracu.ac.bd

Md. Fahmid-Ul-Alam Juboraj[†]

Department of Computer Science and Engineering
BRAC University
Dhaka 1212, Bangladesh
fahmid.juboraj@bracu.ac.bd

Swakkhar Shatabda

Department of Computer Science and Engineering
BRAC University
Dhaka 1212, Bangladesh
swakkhar.shatabda@bracu.ac.bd

February 25, 2026

ABSTRACT

Pro-inflammatory peptides (PIPs) play critical roles in immune signaling and inflammation but are difficult to identify experimentally due to costly and time-consuming assays. To address this challenge, we present **KEMP-PIP**, a hybrid machine learning framework that integrates deep protein embeddings with handcrafted descriptors for robust PIP prediction. Our approach combines contextual embeddings from pretrained ESM protein language models with multi-scale k-mer frequencies, physicochemical descriptors, and modLAMP sequence features. Feature pruning and class-weighted logistic regression manage high dimensionality and class imbalance, while ensemble averaging with an optimized decision threshold enhances the sensitivity–specificity balance. Through systematic ablation studies, we demonstrate that integrating complementary feature sets consistently improves predictive performance. On the standard benchmark dataset, KEMP-PIP achieves an MCC of 0.505, accuracy of 0.752, and AUC of 0.762, outperforming ProIn-fuse, MultiFeatVotPIP, and StackPIP. Relative to StackPIP, these results represent improvements of 9.5% in MCC and 4.8% in both accuracy and AUC. The KEMP-PIP web server is freely available at <https://nilsparrow1920-kemp-pip.hf.space/> and the full implementation at <https://github.com/S18-Niloy/KEMP-PIP>.

[†]These authors contributed equally to this work.

Keywords pro-inflammatory peptides · protein language models · ESM embeddings · k-mer features · ensemble learning · logistic regression

1 Introduction

Pro-inflammatory peptides (PIPs) are short amino acid chains that promote inflammation by activating immune responses. They function as cytokines or chemokines—signaling molecules that recruit immune cells to sites of infection or injury, enhance pathogen clearance, and stimulate the production of further pro-inflammatory mediators. Excessive production or unregulated activity of PIPs, however, can lead to tissue damage, chronic inflammation, and the pathology of numerous inflammatory and autoimmune diseases [1]. Notable examples include fragments derived from IL-1 β , which directly promote inflammation and immune cell activation [1].

PIPs share a characteristic set of physicochemical features. They are typically enriched in positively charged residues (lysine, arginine) that facilitate electrostatic interactions with negatively charged cell membranes and immune receptors. Their amphipathic nature [2]—arising from the spatial segregation of hydrophobic and hydrophilic residues—enables membrane insertion and receptor binding, effects further reinforced by moderate hydrophobicity [3] and a high hydrophobic moment. Structural preferences for α -helical or β -sheet conformations stabilize functional motifs, while their compact size (10–50 residues) confers flexibility. Resistance to proteolytic degradation prolongs their activity in inflammatory environments, and aggregation propensity can amplify immune stimulation. Collectively, charge, hydrophobicity, amphipathicity, secondary structure, size, and stability define the pro-inflammatory potential of a bioactive peptide.

Experimentally, PIPs are identified by exposing immune cells or animal models to candidate peptides and measuring downstream inflammatory responses—cytokine release, cell activation, or tissue inflammation [4]. Such assays are labor-intensive, expensive, and low-throughput, making computational prediction an attractive complement. From a machine learning perspective [5], PIP prediction presents four interrelated challenges: (i) the sequence–activity relationship is governed by subtle motifs and residue preferences (e.g., enrichment in A, F, I, L, V) that are not obvious in raw sequence data; (ii) validated datasets are small and class-imbalanced, with non-PIPs outnumbering PIPs, biasing naive classifiers; (iii) immunogenicity depends on physicochemical, structural, and evolutionary factors that must all be encoded as informative features; and (iv) models must generalize to held-out sequences, demanding careful regularization, feature selection, and ensemble design.

Several dedicated computational tools have addressed these challenges, including ProInflam [1], ProIn-Fuse [6], MultiFeatVotPIP [7], PIP-EL [8], and StackPIP [9]. These methods exploit descriptors ranging from amino acid composition and dipeptide frequencies to evolutionary profiles and motif patterns, paired with support vector machines, random forests, and voting ensembles. Yet biologically interpretable, therapeutically applicable predictions remain elusive. MultiFeatVotPIP, for example, achieves competitive accuracy but relies on numerous potentially redundant hand-crafted features that can overfit imbalanced data, applies unweighted voting that ignores classifier-specific error profiles, and reports primarily internal validation results that complicate generalization claims.

We address these gaps with **KEMP-PIP**, a lightweight hybrid framework that fuses (i) contextual sequence representations from the pretrained ESM2 protein language model, (ii) multi-scale k-mer frequency vectors encoding local motif patterns, and (iii) physicochemical and modLAMP global descriptors. Two complementary feature sets train separate class-weighted logistic regression classifiers whose probability outputs are ensemble-averaged with an MCC-optimized threshold. KEMP-PIP surpasses all compared baselines across every reported metric while remaining computationally affordable and accessible via a public web server.

Contributions.

- A lightweight hybrid architecture combining pretrained protein language model embeddings with multi-scale handcrafted descriptors, achieving state-of-the-art PIP classification performance.
- A systematic ablation covering individual features, four classifier families, and all pairwise two-model ensembles with jointly tuned mixing weights and decision thresholds.
- A freely accessible web server accepting FASTA files, CSV files, and manual input, enabling the wider bioinformatics community to deploy KEMP-PIP without programming expertise.

2 Data Construction

Source and preprocessing. The dataset originates from the MultiFeatVotPIP benchmark repository [7]. Raw sequences were preprocessed by removing duplicates and entries containing non-standard amino acids, and all characters were normalized to uppercase with no gaps or special characters. CD-HIT was applied at a sequence identity threshold of 0.60 to reduce redundancy. Table 1 summarizes the resulting splits. The positive class (PIPs) constitutes approximately 43% of training samples, introducing mild class imbalance that is addressed explicitly during model training.

Table 1: Dataset composition after preprocessing and redundancy reduction. PIP: pro-inflammatory; n-PIP: non-pro-inflammatory.

| PIP (train) | n-PIP (train) | PIP (test) | n-PIP (test) |
|-------------|---------------|------------|--------------|
| 1,245 | 1,627 | 171 | 171 |

Task formulation. Given a peptide sequence $s \in \mathcal{A}^*$ over the standard 20-letter amino acid alphabet \mathcal{A} , the task is binary classification: predict whether s exhibits pro-inflammatory activity. We treat this as a supervised learning problem with probabilistic output calibrated by an MCC-optimized threshold.

3 Methodology

The overall workflow is illustrated in Figure 1. Feature extraction produces four complementary representations that are fused into two model inputs. After zero-variance filtering and coefficient-magnitude pruning, two logistic regression classifiers are trained and their outputs combined by probability averaging. The resulting system is deployed as a public web server.

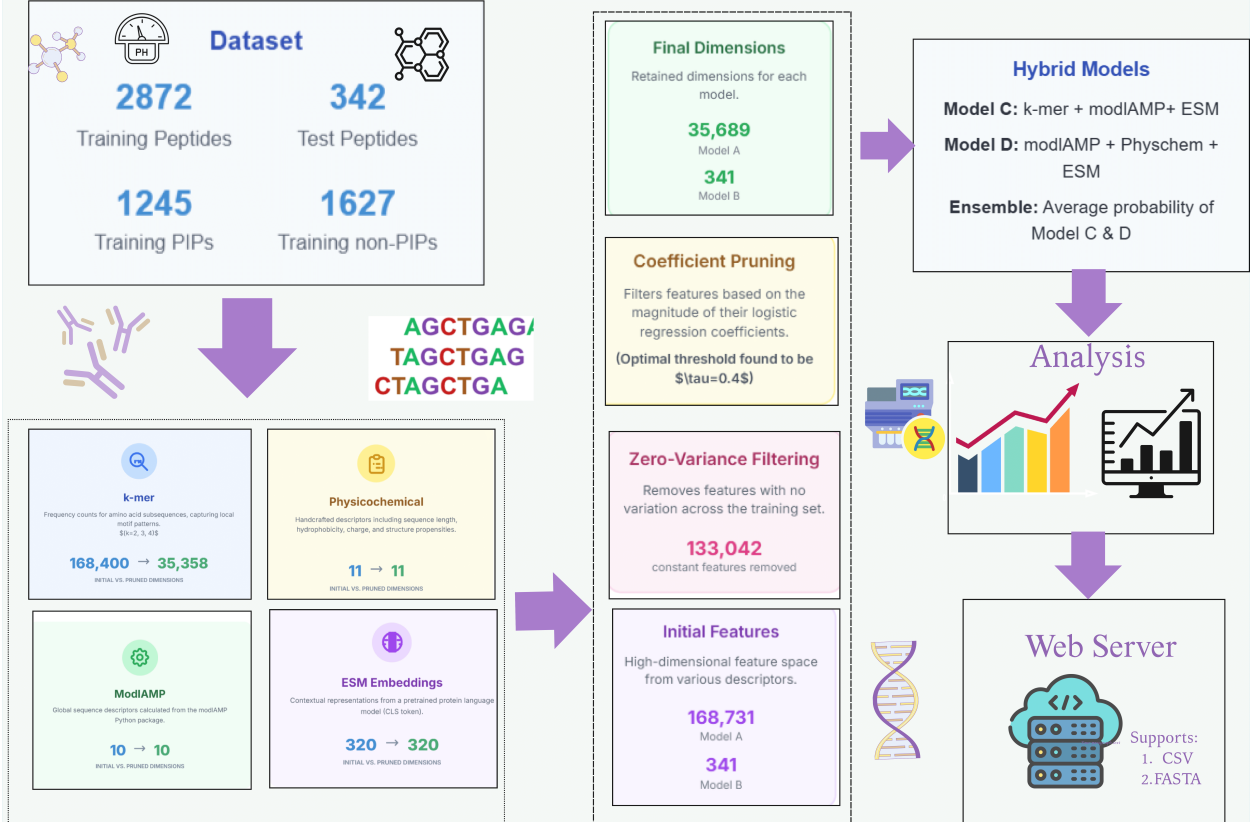


Figure 1: Architecture of the KEMP-PIP framework. Four feature streams are fused into two hybrid models whose predictions are ensemble-averaged with a tuned threshold.

3.1 Feature Extraction

Multi-scale k-mer frequencies. For a peptide s of length L , we compute normalized k-mer frequencies [10] for $k \in \{2, 3, 4\}$:

$$f_{i,j}^{(k)} = \frac{c_{i,j}}{\sum_m c_{i,m}}, \quad (1)$$

where $c_{i,j}$ is the count of the j -th k -mer in sequence i . Feature dimensions are $20^2 = 400$, $20^3 = 8,000$, and $20^4 = 160,000$, giving a concatenated vector $\mathbf{X}_{\text{kmer}} \in \mathbb{R}^{N \times 168,400}$.

Physicochemical descriptors. We encode 11 handcrafted descriptors per peptide: (1) sequence length L ; (2) mean Kyte–Doolittle hydrophobicity [11]; (3–4) helical and sheet hydrophobic moments (Eisenberg, $\theta = 100^\circ$ and 180°) [12]; (5–6) positive charge Q^+ and charge density ρ^+ at pH 7 [13]; (7–8) helix- and sheet-propensity fractions [14]; and (9–11) trypsin, chymotrypsin, and elastase cleavage-site densities [15]. The full physicochemical feature matrix is $\mathbf{X}_{\text{pc}} \in \mathbb{R}^{N \times 11}$.

ModIAMP global descriptors. We use the modIAMP Python package [16] to compute $D = 10$ global sequence descriptors per peptide, yielding $\mathbf{X}_{\text{modIAMP}} \in \mathbb{R}^{N \times 10}$.

ESM protein language model embeddings. We use the pretrained ESM2-T6-8M (UR50D) transformer [17]. Each peptide is tokenized at the residue level and passed through the encoder; the [CLS] token representation from the final hidden layer [18] provides a fixed-length global embedding:

$$\mathbf{z}_i \in \mathbb{R}^{320}. \quad (2)$$

Unlike handcrafted descriptors, these embeddings capture deep contextual dependencies learned from millions of protein sequences.

Table 2 summarizes all feature types, original dimensionalities, and post-pruning sizes.

Table 2: Feature descriptor summary. Pruning applies only to k-mer features via zero-variance filtering; all other features are retained in full.

| Feature Type | Description | Original Dim. | Pruned Dim. |
|------------------------|---|---------------|-------------|
| Multi-scale k-mer | Normalized frequencies, $k \in \{2, 3, 4\}$ | 168,400 | 35,358 |
| Physicochemical | Hydrophobicity, charge, cleavage densities | 11 | 11 |
| ModIAMP | Global sequence descriptors | 10 | 10 |
| ESM embeddings | CLS token, ESM2-T6-8M | 320 | 320 |
| Model C (fused) | k-mer + ModIAMP + ESM | 168,730 | 35,688 |
| Model D (fused) | Physicochemical + ModIAMP + ESM | 341 | 341 |

3.2 Feature Pruning

The initial feature space of Model C is extremely high-dimensional (168,730 variables), necessitating a two-stage pruning strategy [19].

Stage 1 — Zero-variance filtering. Features that are constant across all training sequences (i.e., zero variance) are discarded. This step is critical for sparse k-mer encodings in which many k -mers never appear in the corpus [20]. After filtering, Model C is reduced from 168,730 to **35,688** features (133,042 constant features removed). Model D retains all 341 features.

Stage 2 — Coefficient-magnitude pruning. A class-weighted logistic regression is trained on the filtered features, and features are ranked by $|\hat{\beta}_j|$ [21]. A threshold grid $\tau \in \{0, 10^{-6}, 5 \times 10^{-6}, \dots, 10^{-3}\}$ is evaluated; for each τ only features with $|\hat{\beta}_j| \geq \tau$ are retained, a model is re-trained, and MCC on a stratified 10% validation split serves as the selection criterion. The optimal threshold for both models is $\tau = 0$, confirming that retaining all non-constant features maximizes validation MCC and that the major dimensionality reduction is achieved by Stage 1 alone.

3.3 Feature Combination and Ensemble Learning

Two complementary feature matrices are constructed and independently standardized:

$$\mathbf{X}_C = [\mathbf{X}_{\text{kmer}} \mid \mathbf{X}_{\text{modIAMP}} \mid \mathbf{X}_{\text{ESM}}] \in \mathbb{R}^{N \times 35,688}, \quad (3)$$

$$\mathbf{X}_D = [\mathbf{X}_{\text{pc}} \mid \mathbf{X}_{\text{modIAMP}} \mid \mathbf{X}_{\text{ESM}}] \in \mathbb{R}^{N \times 341}. \quad (4)$$

A class-weighted logistic regression [23] with the L-BFGS solver [24] is trained on each matrix. Class weights are set inversely proportional to class frequencies to counteract the PIP/non-PIP imbalance.

Ensemble predictions are obtained by averaging the two models’ predicted probabilities with a tunable mixing coefficient α [25]:

$$P_{\text{ens}} = \alpha P_C + (1 - \alpha) P_D. \quad (5)$$

The final label is assigned by thresholding:

$$\hat{y} = \begin{cases} 1 & P_{\text{ens}} > t, \\ 0 & \text{otherwise.} \end{cases} \quad (6)$$

Both $\alpha \in [0, 1]$ and $t \in (0, 1)$ are jointly optimized on a held-out validation split to maximize MCC [26]. For the primary KEMP-PIP configuration ($C \oplus D$), the optimal values are $\alpha = 0.65$ and $t = 0.36$.

3.4 Performance Metrics

We evaluate all models using five standard bioinformatics classification metrics [28]: Accuracy (ACC), Sensitivity (SN), Specificity (SP), Matthews Correlation Coefficient (MCC) [29], and Area Under the ROC Curve (AUC) [30]:

$$\text{ACC} = \frac{\text{TP} + \text{TN}}{\text{TP} + \text{TN} + \text{FP} + \text{FN}}, \quad \text{SN} = \frac{\text{TP}}{\text{TP} + \text{FN}}, \quad \text{SP} = \frac{\text{TN}}{\text{TN} + \text{FP}}, \quad (7)$$

$$\text{MCC} = \frac{\text{TP} \cdot \text{TN} - \text{FP} \cdot \text{FN}}{\sqrt{(\text{TP} + \text{FP})(\text{TP} + \text{FN})(\text{TN} + \text{FP})(\text{TN} + \text{FN})}}. \quad (8)$$

MCC is the primary selection criterion throughout because it provides a balanced summary of classification performance under class imbalance, penalizing both false positives and false negatives.

4 Results and Analysis

4.1 Feature Ablation

Table 3 reports MCC, AUC, and ACC on both the validation split and the independent test set for each individual feature type and multi-feature combination. The best value in each column is bolded.

Table 3: Feature ablation study. Best values per column in **bold**.

| Feature Combination | Dim. | Validation | | | Test | | |
|---|--------|---------------|---------------|---------------|---------------|---------------|---------------|
| | | MCC | AUC | ACC | MCC | AUC | ACC |
| <i>Individual feature sets</i> | | | | | | | |
| k-mer | 35,358 | 0.2391 | 0.6868 | 0.6319 | 0.3351 | 0.7592 | 0.6608 |
| Physicochemical | 11 | 0.0879 | 0.6360 | 0.5035 | 0.1451 | 0.6438 | 0.5643 |
| ESM | 320 | 0.1797 | 0.6009 | 0.5660 | 0.2026 | 0.6577 | 0.5994 |
| modlAMP | 10 | 0.1658 | 0.6432 | 0.5382 | 0.1461 | 0.6538 | 0.5643 |
| <i>Two-feature combinations</i> | | | | | | | |
| k-mer + Physchem | 35,369 | 0.2401 | 0.6912 | 0.6319 | 0.3704 | 0.7682 | 0.6784 |
| k-mer + ESM | 35,678 | 0.2807 | 0.6997 | 0.6493 | 0.3486 | 0.7755 | 0.6667 |
| k-mer + modlAMP | 35,368 | 0.2546 | 0.6921 | 0.6389 | 0.3735 | 0.7739 | 0.6813 |
| <i>Three- and four-feature combinations</i> | | | | | | | |
| k-mer + Physchem + ESM | 35,689 | 0.2873 | 0.7034 | 0.6528 | 0.3771 | 0.7809 | 0.6813 |
| k-mer + ESM + modlAMP | 35,688 | 0.2818 | 0.7047 | 0.6493 | 0.3704 | 0.7834 | 0.6784 |
| k-mer + Physchem + ESM + modlAMP | 35,699 | 0.2807 | 0.7070 | 0.6493 | 0.4042 | 0.7876 | 0.6959 |

Several trends are apparent. First, k-mer features carry the strongest standalone signal, reflecting the importance of local sequence composition for proinflammatory activity. Second, every additional descriptor—physicochemical, ESM, or modlAMP—provides a consistent incremental gain, confirming that the four feature types are complementary rather than redundant. Third, the best validation configuration (kmer+physchem+ESM, MCC 0.2873) differs from the best test configuration (kmer+physchem+ESM+modlAMP, MCC 0.4042), suggesting that the validation split is conservative and that the full four-feature fusion generalizes most robustly to unseen data.

4.2 Model Ablation Across Classifiers

Table 4 evaluates the same feature combinations using four alternative classifiers—XGBoost, Random Forest (RF), Support Vector Machine (SVM), and Multi-Layer Perceptron (MLP)—to assess whether the feature-fusion gains are classifier-agnostic.

Table 4: Feature ablation across four classifiers on the independent test set. Best MCC per row in **bold**. Abbreviations: k = k-mer, p = physicochemical, m = modlAMP, e = ESM.

| Feature Set | XGBoost | | | RF | | | SVM | | | MLP | | |
|-------------|---------------|--------|--------|---------------|--------|--------|---------|--------|--------|---------------|--------|--------|
| | MCC | AUC | ACC | MCC | AUC | ACC | MCC | AUC | ACC | MCC | AUC | ACC |
| k | 0.2761 | 0.6973 | 0.6374 | 0.2458 | 0.7325 | 0.6228 | -0.0524 | 0.3909 | 0.4825 | 0.3107 | 0.7575 | 0.6491 |
| p | 0.1530 | 0.6202 | 0.5760 | 0.1588 | 0.6487 | 0.5789 | 0.1230 | 0.5990 | 0.5614 | 0.0946 | 0.6266 | 0.5468 |
| m | 0.3275 | 0.7093 | 0.6637 | 0.2807 | 0.7061 | 0.6404 | 0.2515 | 0.6464 | 0.6257 | 0.2111 | 0.6706 | 0.6023 |
| e | 0.1463 | 0.6141 | 0.5731 | 0.1859 | 0.6239 | 0.5906 | 0.2132 | 0.6433 | 0.6053 | 0.2281 | 0.6417 | 0.6140 |
| k+p | 0.3047 | 0.7244 | 0.6520 | 0.2411 | 0.7033 | 0.6199 | -0.0432 | 0.3931 | 0.4854 | 0.2414 | 0.7222 | 0.5994 |
| k+m | 0.2870 | 0.7134 | 0.6433 | 0.2781 | 0.7194 | 0.6374 | -0.0432 | 0.3940 | 0.4854 | 0.4219 | 0.7561 | 0.7105 |
| k+e | 0.1696 | 0.6267 | 0.5848 | 0.1460 | 0.6267 | 0.5702 | -0.0778 | 0.4046 | 0.4737 | 0.3100 | 0.7399 | 0.6550 |
| p+m | 0.1872 | 0.6586 | 0.5936 | 0.2515 | 0.6940 | 0.6257 | 0.1758 | 0.6202 | 0.5877 | 0.1770 | 0.6420 | 0.5877 |
| p+e | 0.2460 | 0.6638 | 0.6228 | 0.1845 | 0.6532 | 0.5906 | 0.2003 | 0.6473 | 0.5994 | 0.1943 | 0.6258 | 0.5965 |
| m+e | 0.2176 | 0.6570 | 0.6082 | 0.1763 | 0.6569 | 0.5877 | 0.2007 | 0.6488 | 0.5994 | 0.2311 | 0.6487 | 0.6082 |
| k+p+m | 0.2515 | 0.7159 | 0.6257 | 0.2532 | 0.7009 | 0.6257 | -0.0425 | 0.3962 | 0.4854 | 0.2762 | 0.7543 | 0.6316 |
| k+p+e | 0.2466 | 0.6815 | 0.6228 | 0.2105 | 0.6489 | 0.6023 | -0.0699 | 0.4061 | 0.4766 | 0.1410 | 0.7535 | 0.5380 |
| k+m+e | 0.2526 | 0.6798 | 0.6257 | 0.1553 | 0.6585 | 0.5760 | -0.0605 | 0.4072 | 0.4795 | 0.1669 | 0.7423 | 0.5409 |
| p+m+e | 0.2404 | 0.6562 | 0.6199 | 0.2663 | 0.6665 | 0.6316 | 0.2121 | 0.6511 | 0.6053 | 0.2285 | 0.6512 | 0.6140 |
| k+p+m+e | 0.2281 | 0.6703 | 0.6140 | 0.1974 | 0.6540 | 0.5965 | -0.0686 | 0.4092 | 0.4766 | 0.2713 | 0.7192 | 0.6199 |

The SVM consistently underperforms with k-mer features due to the high dimensionality of the input, often yielding negative MCC values—a known failure mode of kernel SVMs on ultra-sparse, high-dimensional data without specialized preprocessing. XGBoost and the MLP show the greatest benefit from feature fusion, with the MLP achieving the highest single-model MCC of 0.4219 on k+m. Across classifiers, modlAMP exhibits surprisingly strong standalone performance (XGBoost MCC 0.3275), highlighting the value of global sequence descriptors even without deep embeddings.

4.3 Ensemble Ablation

To identify the optimal two-model combination, we trained five single logistic regression models on the following feature sets:

- kmer + physchem + ESM

- kmer + physchem + modLAMP

- kmer + ESM + modLAMP

- physchem + ESM + modLAMP

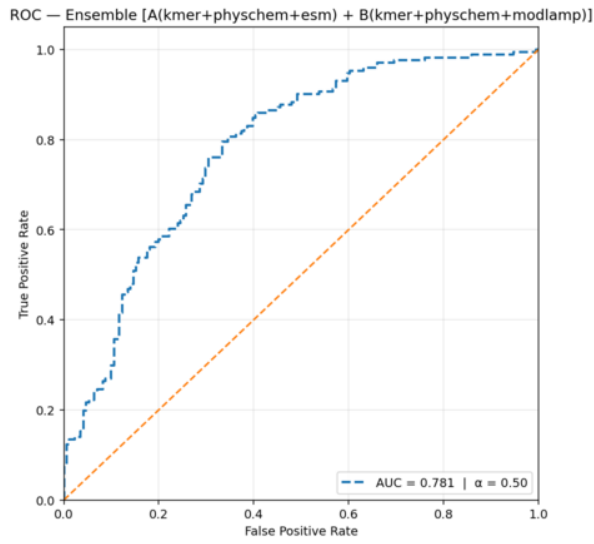
- kmer + physchem + ESM + modLAMP

All ten pairwise ensembles were formed by linearly blending predicted probabilities with weight $\alpha \in [0, 1]$, and both α and the decision threshold t were jointly optimized to maximize MCC on the held-out validation split.

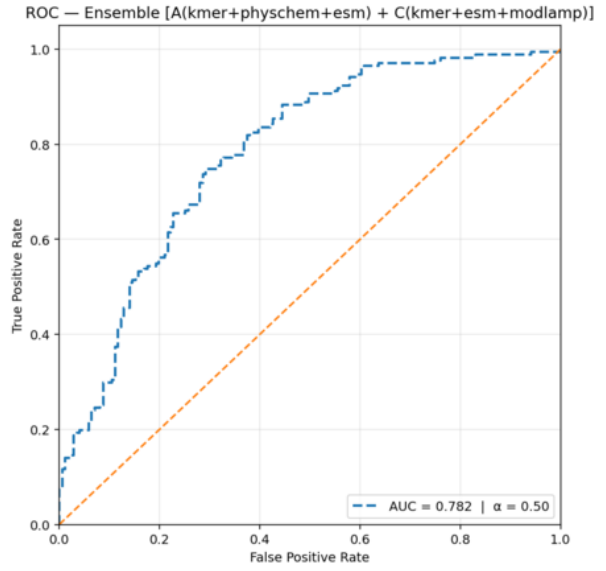
Table 5: Performance of pairwise ensembles with optimized α and threshold t . Best value per column in **bold**. \oplus denotes ensemble averaging.

| Ensemble | α | t | ACC | AUC | MCC | F1 | SN | SP |
|--------------------------------|-------------|-------------|---------------|---------------|---------------|---------------|---------------|---------------|
| A \oplus B | 0.10 | 0.10 | 0.7339 | 0.7787 | 0.4738 | 0.7534 | 0.8129 | 0.6550 |
| A \oplus C | 0.00 | 0.17 | 0.7251 | 0.7834 | 0.4508 | 0.7314 | 0.7485 | 0.7018 |
| A \oplus D | 0.60 | 0.37 | 0.7456 | 0.7585 | 0.4922 | 0.7372 | 0.7135 | 0.7778 |
| A \oplus E | 0.00 | 0.18 | 0.7281 | 0.7876 | 0.4565 | 0.7335 | 0.7485 | 0.7076 |
| B \oplus C | 0.55 | 0.11 | 0.7368 | 0.7820 | 0.4784 | 0.7541 | 0.8070 | 0.6667 |
| B \oplus D | 0.95 | 0.10 | 0.7398 | 0.7750 | 0.4912 | 0.7652 | 0.8480 | 0.6316 |
| B \oplus E | 0.90 | 0.10 | 0.7368 | 0.7792 | 0.4793 | 0.7554 | 0.8129 | 0.6608 |
| C \oplus D | 0.65 | 0.36 | 0.7515 | 0.7617 | 0.5049 | 0.7401 | 0.7076 | 0.7953 |
| C \oplus E | 0.15 | 0.17 | 0.7281 | 0.7873 | 0.4568 | 0.7350 | 0.7544 | 0.7018 |
| D \oplus E | 0.40 | 0.37 | 0.7485 | 0.7620 | 0.4979 | 0.7410 | 0.7193 | 0.7778 |

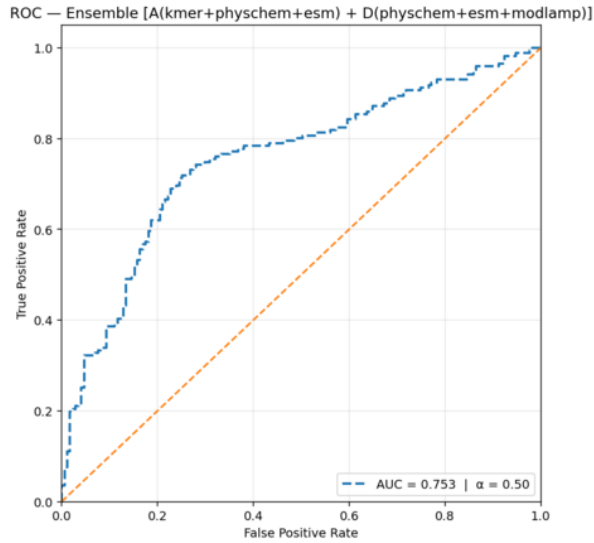
Table 5 shows that no single ensemble dominates on all metrics, reflecting the well-known trade-off between sensitivity and specificity. The **C \oplus D** ensemble achieves the best overall balance, leading on ACC (0.7515), MCC (0.5049), and SP (0.7953); it is therefore selected as the primary KEMP-PIP configuration. The **A \oplus C** ensemble achieves the highest AUC (0.7834), making it preferable when ranking-based evaluation is paramount. The **B \oplus D** ensemble leads on F1 (0.7652) and SN (0.8480), making it the most appropriate choice when minimizing false negatives is the priority (e.g., clinical screening). ROC curves for all ten pairwise ensembles are displayed in Figure 3.



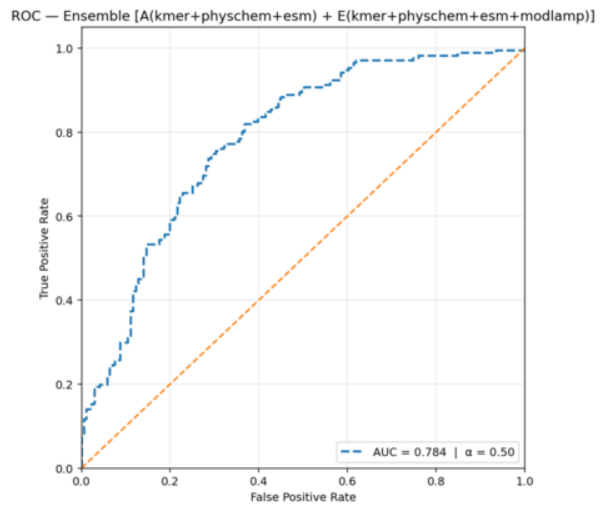
(a) $A \oplus B$



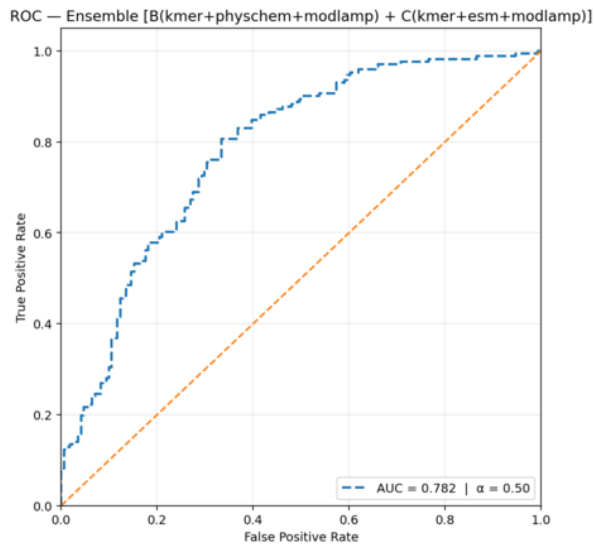
(b) $A \oplus C$



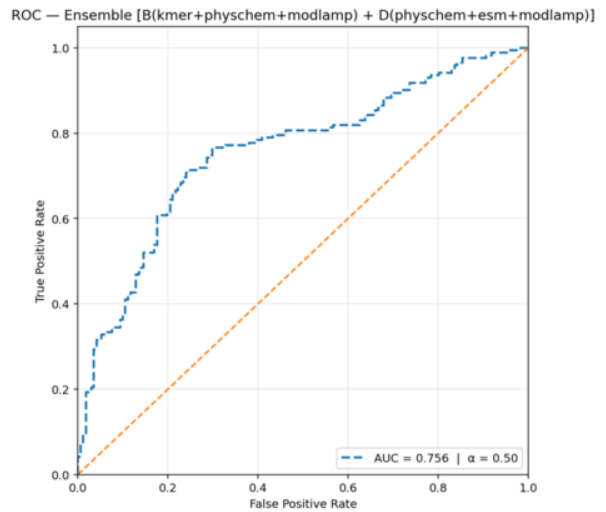
(c) $A \oplus D$



(d) $A \oplus E$



(e) $B \oplus C$



(f) $B \oplus D$

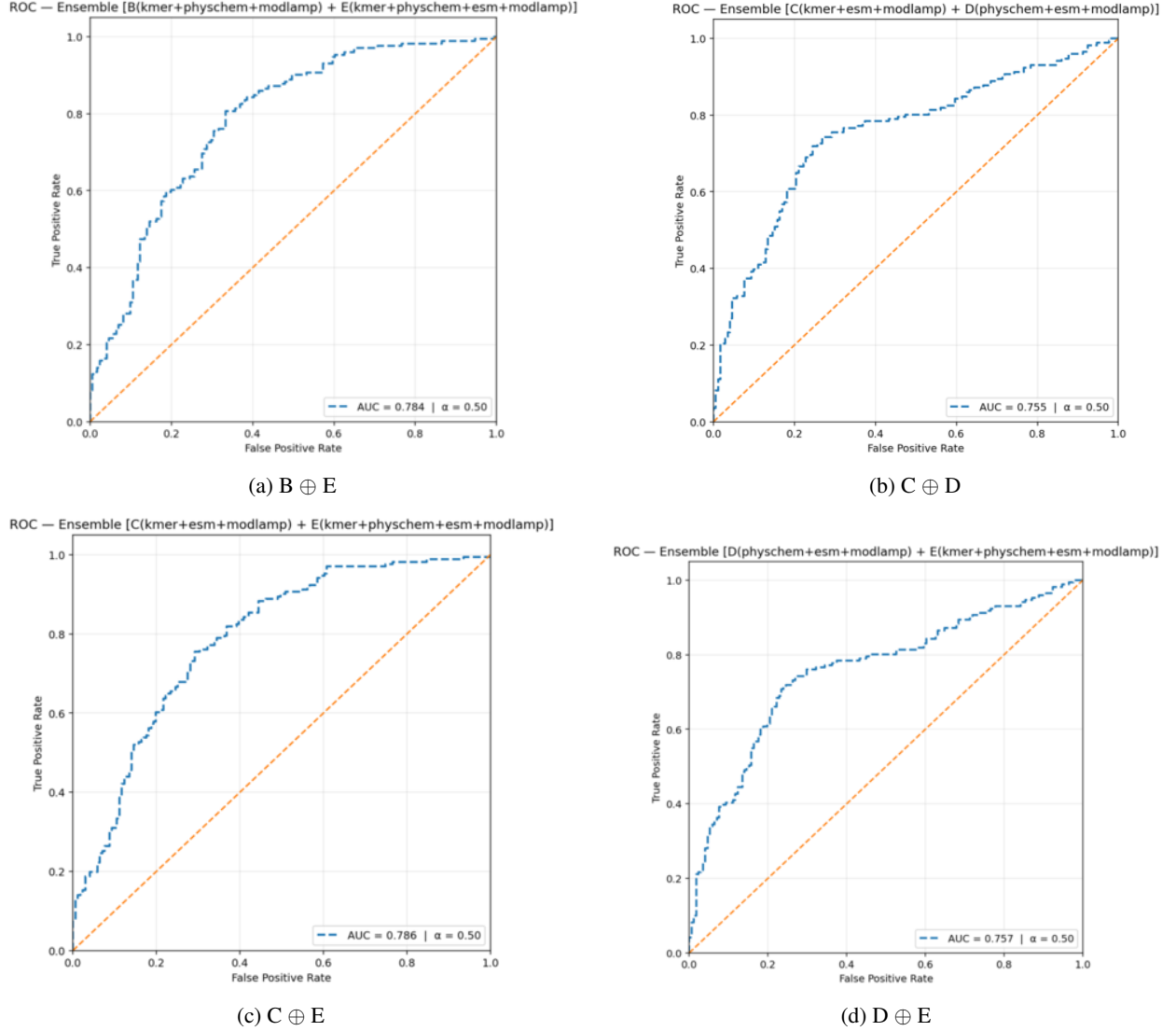


Figure 3: ROC curves for ensemble combinations (a)–(j).

4.4 Comparison with State-of-the-Art Methods

Table 6 compares KEMP-PIP (C⊕D configuration) against ProIn-fuse, MultiFeatVotPIP, and StackPIP on the independent test set. KEMP-PIP achieves the highest value on every reported metric.

Table 6: Independent test-set comparison. Best scores in **bold**.

| Method | SN | SP | ACC | AUC | MCC |
|-----------------|--------------|--------------|--------------|--------------|--------------|
| ProIn-fuse | 0.502 | 0.736 | 0.619 | 0.704 | 0.246 |
| MultiFeatVotPIP | 0.521 | 0.790 | 0.655 | 0.686 | 0.322 |
| StackPIP | 0.628 | 0.731 | 0.704 | 0.714 | 0.410 |
| KEMP-PIP | 0.708 | 0.795 | 0.752 | 0.762 | 0.505 |

Relative to the previous best method (StackPIP), KEMP-PIP improves MCC by 9.5% and both accuracy and AUC by 4.8%. It also improves sensitivity by 12.7 percentage points while simultaneously improving specificity by 8.8 percentage points—a combination rarely achieved, since sensitivity and specificity are typically in tension. This balanced gain reflects the effectiveness of the ensemble design and MCC-based threshold optimization.

Web server. To maximize accessibility, we developed a user-friendly web server (Figure 4) accepting peptide sequences in FASTA or plain text format and returning per-sequence probability scores and binary classification labels. The server requires no programming expertise and is freely available at <https://nilsparrow1920-kemp-pip.hf.space/>.

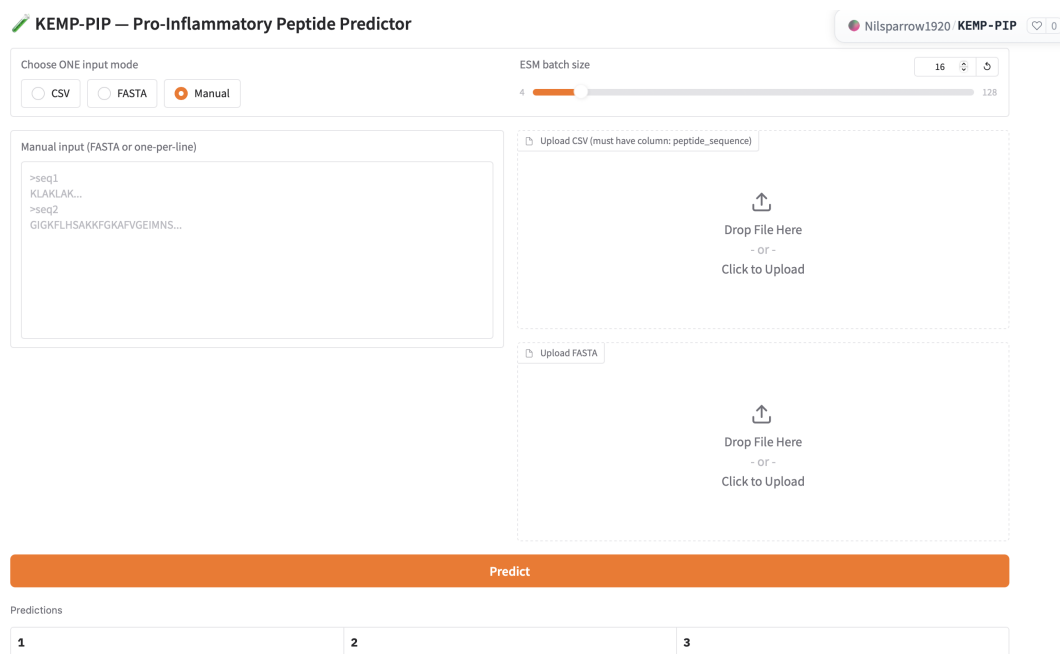


Figure 4: Web interface of the KEMP-PIP framework, supporting FASTA file upload, CSV upload, and manual sequence entry.

5 Conclusion

We presented KEMP-PIP, a feature-fusion machine learning framework for the binary classification of pro-inflammatory peptides. By fusing contextual ESM transformer embeddings with multi-scale k-mer frequencies, physicochemical indices, and modLAMP global descriptors, the framework captures complementary sequence signals—from fine-grained local motifs to global biophysical properties and learned evolutionary context—that individually fail to characterize pro-inflammatory activity fully. Zero-variance filtering and coefficient-based pruning reduce the feature space efficiently, class-weighted logistic regression counteracts label imbalance, and jointly optimized ensemble averaging balances sensitivity and specificity without sacrificing either. KEMP-PIP surpasses ProIn-fuse, MultiFeatVotPIP, and StackPIP across all five evaluated metrics on the independent test set.

Limitations remain. The training corpus, though curated and de-redundified, may not fully represent the sequence and structural diversity of PIPs across organisms. Future directions include expanding the dataset to cover taxonomically diverse peptides, incorporating three-dimensional structural descriptors from predicted protein structures, and exploring larger pretrained language models (e.g., ESM2-3B) or fine-tuning strategies tailored to immunological data. Integrating KEMP-PIP into automated peptide design pipelines could further accelerate the discovery of therapeutic candidates.

Author contributions. Soumik Deb Niloy: Methodology, Software, Investigation, Writing – Original Draft. Md. Fahmid-Ul-Alam Juboraj: Methodology, Formal Analysis, Investigation, Writing – Original Draft. Swakkhar Shatabda: Conceptualization, Supervision, Writing – Review & Editing.

Data and code availability. The dataset is publicly available at <https://github.com/ChaoruiYan019/MultiFeatVotPIP>. Source code and web server: <https://github.com/S18-Niloy/KEMP-PIP> and <https://nilsparrow1920-kemp-pip.hf.space/>.

References

- [1] S. Gupta, P. Kapoor, K. Chaudhary, A. Gautam, R. Kumar, Open Source Drug Discovery Consortium, and G. P. S. Raghava. ProInflam: A webservice for the prediction of proinflammatory antigenicity of peptides and proteins. *Journal of Translational Medicine*, 14:1–12, 2016.

- [2] E. Pérez-Payá, R. A. Houghten, and S. E. Blondelle. The role of amphipathicity in the folding, self-association and biological activity of multiple subunit small proteins. *Journal of Biological Chemistry*, 270(3):1048–1056, 1995.
- [3] C. Zhu, Y. Gao, H. Li, S. Meng, and L. Li. Characterizing hydrophobicity of amino acid side chains in a protein environment via measuring contact angle of a water nanodroplet on planar peptide network. *Proceedings of the National Academy of Sciences*, 2015.
- [4] P. Mukherjee, S. Roy, D. Ghosh, and S. K. Nandi. Role of animal models in biomedical research: a review. *Laboratory Animal Research*, 38:18, 2022.
- [5] A. Raza, J. Uddin, S. Akbar, F. K. Alarfaj, Q. Zou, and A. Ahmad. Comprehensive analysis of computational methods for predicting anti-inflammatory peptides. *Archives of Computational Methods in Engineering*, 31:3211–3229, 2024.
- [6] M. Khatun, M. M. Hasan, W. Shoombuatong, and H. Kurata. ProIn-Fuse: Improved and robust prediction of proinflammatory peptides by fusing of multiple feature representations. *Journal of Computer-Aided Molecular Design*, 34(12):1229–1236, 2020.
- [7] C. Yan, A. Geng, Z. Pan, Z. Zhang, and F. Cui. MultiFeatVotPIP: A voting-based ensemble learning framework for predicting proinflammatory peptides. *Briefings in Bioinformatics*, 25(6):bbae505, 2024.
- [8] B. Manavalan, T. H. Shin, M. O. Kim, and G. Lee. PIP-EL: A new ensemble learning method for improved proinflammatory peptide predictions. *Frontiers in Immunology*, 9:1783, 2018.
- [9] L. Yao, F. Wang, P. Xie, J. Guan, Z. Zhao, X. He, X. Liu, Y.-C. Chiang, and T.-Y. Lee. StackPIP: An effective computational framework for accurate and balanced identification of proinflammatory peptides. *Journal of Chemical Information and Modeling*, 65(14):7777–7788, 2025.
- [10] K. M. Jenike, L. Campos-Domínguez, M. Boddé, J. Cerca, C. N. Hodson, M. C. Schatz, and K. S. Jaron. Guide to k-mer approaches for genomics across the tree of life. arXiv:2404.01519, 2024.
- [11] F. Waibl, M. L. Fernández-Quintero, F. S. Wedl, et al. Comparison of hydrophobicity scales for predicting biophysical properties of antibodies. *Frontiers in Molecular Biosciences*, 9:960194, 2022.
- [12] D. Eisenberg, R. M. Weiss, T. C. Terwilliger, and W. Wilcox. Hydrophobic moments and protein structure. *Faraday Discussions of the Chemical Society*, 17:109–120, 1982.
- [13] B. F. Shaw, H. Arthanari, M. Narovlyansky, et al. Neutralizing positive charges at the surface of a protein lowers its rate of amide hydrogen exchange without altering its structure or increasing its thermostability. *Journal of the American Chemical Society*, 132(49):17411–17425, 2010.
- [14] C. O. Mackenzie and G. Grigoryan. Protein structural motifs in prediction and design. *Current Opinion in Structural Biology*, 44:161–167, 2017.
- [15] H. Sun, B. Qiao, W. Choi, et al. Origin of proteolytic stability of peptide-brush polymers as globular proteomimetics. *ACS Central Science*, 7(12):2063–2072, 2021.
- [16] A. T. Müller, G. Gabernet, J. A. Hiss, and G. Schneider. modLAMP: Python for antimicrobial peptides. *Bioinformatics*, 33(17):2753–2755, 2017.
- [17] K. Zheng, S. Long, T. Lu, J. Yang, X. Dai, M. Zhang, Z. Nie, W.-Y. Ma, and H. Zhou. ESM all-atom: Multi-scale protein language model for unified molecular modeling. arXiv:2403.12995, 2024.
- [18] R. Seoh, H.-S. Chang, and A. McCallum. Encoding multi-domain scientific papers by ensembling multiple CLS tokens. arXiv:2309.04333, 2023.
- [19] Y. Ye, H. Zhou, J. Cai, et al. Dynamic feature pruning and consolidation for occluded person re-identification. arXiv:2211.14742, 2022.
- [20] Y.-H. Xiao, L. Huang, D. Ramírez, C. Qian, and H. C. So. One-bit covariance reconstruction with non-zero thresholds. arXiv:2303.16455, 2023.
- [21] M. Sun, Z. Liu, A. Bair, and J. Z. Kolter. A simple and effective pruning approach for large language models. In *Proceedings of ICLR 2024*. arXiv:2306.11695, 2024.
- [22] L. Gao and L. Guan. Interpretability of machine learning: Recent advances and future prospects. arXiv:2305.00537, 2023.
- [23] N. Abbood, J. Effert, K. A. J. Bozhueyuek, and H. B. Bode. Guidelines for optimizing type S nonribosomal peptide synthetases. *ACS Synthetic Biology*, 12(8):2432–2443, 2023.
- [24] Y. Niu, Z. Fabian, S. Lee, M. Soltanolkotabi, and S. Avestimehr. mL-BFGS: A momentum-based L-BFGS for distributed large-scale neural network optimization. arXiv:2307.13744, 2023.
- [25] Q. Yang. Blending ensemble for classification with genetic-algorithm generated alpha factors and sentiments (GAS). arXiv:2411.03035, 2024.
- [26] N. Das and M. Chakraborty. Machine learning-driven threshold optimization for wavelet packet denoising in EEG-based mental state classification. *IEEE Access*, 2023.
- [27] P. Greenside, M. Hillenmeyer, and A. Kundaje. Prediction of protein-ligand interactions from paired protein sequence motifs and ligand substructures. *Pacific Symposium on Biocomputing*, 23:20–31, 2018.

- [28] X. Fu, Y. Yuan, H. Qiu, et al. AGF-PPIS: A protein-protein interaction site predictor based on an attention mechanism and graph convolutional networks. *Methods*, 222:142–151, 2024.
- [29] C. Xiao, Z. Zhou, J. She, et al. PEL-PVP: Application of plant vacuolar protein discriminator based on PEFT ESM-2 and bilayer LSTM in an unbalanced dataset. *International Journal of Biological Macromolecules*, 277:134317, 2024.
- [30] Ş. K. Çorbacıoğlu and G. Aksel. Receiver operating characteristic curve analysis in diagnostic accuracy studies: A guide to interpreting the area under the curve value. *Turkish Journal of Emergency Medicine*, 23(4):195–198, 2023.